Metal–Organic Polyhedra Cages Immobilized on a Plasmonic Substrate for Sensitive Detection of Trace Explosives

Chen Wang, Jin Shang, Yue Lan, Tian Tian, Hui Wang, Xi Chen, Jing-Ying Gu, Jefferson Zhe Liu, Li-Jun Wan, Wei Zhu, and Guangtao Li**

A novel strategy for highly sensitive detection and discrimination of explosives is developed based on the metal–organic polyhedra (MOP)-decorated plasmonic substrate. It is found that the careful selection of the geometric and electronic characteristics of the assembly units (organic ligands and unsaturated metals sites) embedded within the MOP cage allows for the integration of multiple weak molecular interactions in a controllable fashion and thus the MOP cage can serve as an excellent receptor for selective uptake and binding of explosives. By further grafting of the MOP cage onto a plasmonic substrate with good surface-enhanced Raman scattering enhancement factor, the resulting sensor shows a good sensing capability to various groups of ultratrace explosives, especially the challenging aliphatic nitro-organics.

1. Introduction

Efficient detection of hidden explosives in war zones, minefield remediation, and counter-terrorism application is a pressing concern.[1] Numerous strategies have been developed to sense three classes of the most commonly used energetic compounds including nitrated aromatics (e.g., TNT and DNT), nitramines (e.g., RDX and HMX), and nitrate esters (e.g., PETN). However, finding a suitable and efficient sensing strategy for directly detecting trace aliphatic nitro-organics, such as RDX, HMX, and PETN, still faces formidable challenges.[2] These challenges arise from the intrinsic property of these explosive molecules, such as ultralow volatility, unfavorable reduction potentials, and poor affinity for sensory materials, due to their highly 3D structure and the lack of π–π interaction. It is thus very difficult to design and synthesize a proper receptor that exhibits high affinities and selectivities toward aliphatic nitro-organics.[3] In addition, since many current sensors are only specific for one class of explosive, which reduces their overall utility, the development of a sensor for broad-class explosive detection also constitutes a serious challenge.[4] Therefore, developing a chemosensor capable of sensitively detecting a broad range of explosives, in particular the aliphatic nitro-organic, is highly desirable.

Metal–organic polyhedra (MOP), discrete molecular cages that are constructed through the coordination of organic linkers and metal ions, have attracted great attentions owing to the well-defined and confined cavity, high symmetry and stability, as well as rich chemical or/and physical properties and functions.[5] Such amazing architectures are derived from modular and high-yield coordination-driven self-assembly method. A careful selection of bridging ligands and metal ions permits to control the well-confined inner space, gated pores, and nanoscale windows. Specifically, the geometric and electronic characteristics that are embedded within the individual assembling components allow for the integration of multiple weak molecular interactions, such as hydrogen bonding, charge–transfer, and brønsted acid–base interaction in a controllable fashion and thus provides specific inner environments for selective uptake and binding of guest molecules.[6] Moreover, the designable exposure of exo-reactive sites around MOP assemblies[7] allows it to further couple with functional substrate such as plasmonic substrate to expand the potential applications. These distinctive features make MOP an excellent candidate for molecular recognition.

Here, we present a novel strategy for detecting broad ultratrace explosives based on a MOP-decorated plasmonic nanohybrid substrate (**Scheme 1**). This strategy features the use of the MOP cage with desired inner space and properties suitable to trap single-explosive molecule (TNT, DNT, RDX, or HMX). The presence of the electron donating sites $-NH_2$ and the unsaturated metal sites Cu^{2+} in the confined cavity enables the integration of multiple molecular interactions, such as charge–transfer and brønsted acid–base interaction, to strengthen the guest–host interactions and thus makes MOP a

C. Wang, Y. Lan, T. Tian, H. Wang, Dr. W. Zhu, Prof. Dr. G. T. Li
Key Lab of Organic Optoelectronic and Molecular Engineering Department of Chemistry
Tsinghua University
Beijing 100084, P.R. China
E-mail: zhuw200461170@163.com; LGT@mail.tsinghua.edu.cn

Dr. J. Shang, X. Chen
Department of Chemical and Biomolecular Engineering
University of Melbourne
Parkville, Victoria 3010, Australia

J.-Y. Gu, Prof. Dr. L.-J. Wan
Institute of Chemistry
Chinese Academy of Sciences (CAS)
Beijing 100190, P.R. China

Prof. J. Z. Liu
Department of Mechanical and Aerospace Engineering
Monash University
Clayton, Victoria 3800, Australia

DOI: 10.1002/adfm.201503071

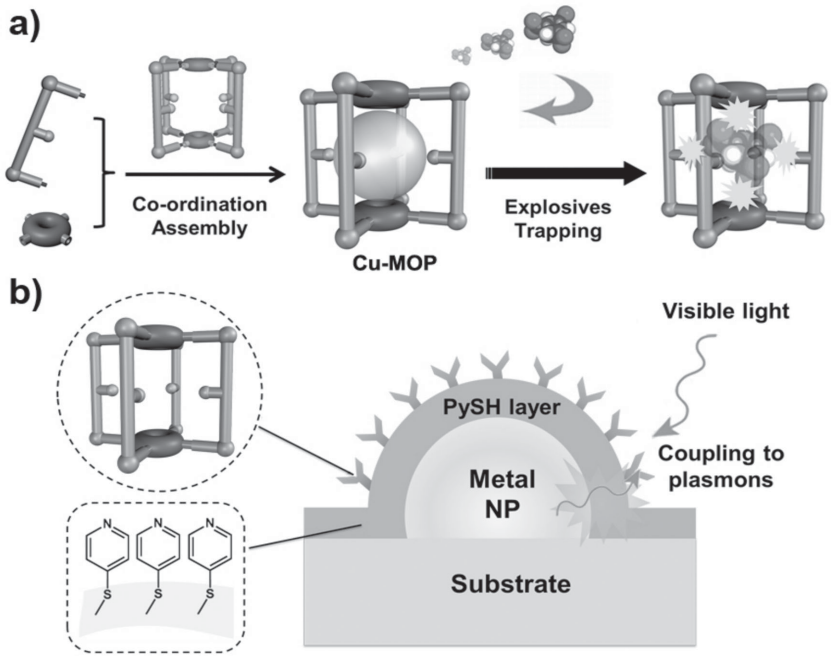

Scheme 1. Schematic illustration of a) the synthesis of the MOP cage with desired inner environment for single-explosive molecule capture, and b) the construction of the MOP-decorated plasmonic substrate for explosive sensing.

good receptor for binding various sorts of explosive molecules, including the challenging aliphatic nitro-organics. Furthermore, the size-exclusion effect derived from the gated pores provides a size- or shape-selectivity for better explosive discrimination. By grafting the MOP onto the Au nanoparticles (NPs)-based plasmonic substrate with good surface-enhanced Raman scattering (SERS) enhancement factors, we found that the resulting MOP-modified or -decorated plasmonic nanohybrids showed a good sensing capability to detect trace explosives. The detection limit for HMX was 10^{-8} M, and for TNT and RDX could be down to 10^{-10} M. Controlled experiments were performed using plasmonic substrate grafted with 4-PySH or $-NH_2$ and showed quite poor sensing behaviors, indicating the formation of a host-stabilized complex in MOP is critical for the good sensing of explosives. Moreover, density functional theory (DFT) computational study was conducted to verify the presence of multiple weak interactions inside MOP at molecular level. In particular, the noncovalent nature of the resulting heteroternary complex indicates that the trapped molecules in the MOP are facilely removable by simply washing, showing an excellent regeneration for real-world application.

2. Results and Discussion

A three-step procedure was employed to construct the MOP-decorated plasmonic nanohybrid substrate. First, the MOP cage was synthesized by slow addition of methanol into a *N,N*-diethyl formamide (DEF) solution of $Cu_2(OAc)_4$ and ligand H_2(2-NH_2-5-i-Pr-3,3′-PBEDDB) (L-NH_2). After 5 d the MOP cage $[Cu_4(L\text{-}NH_2)_4(S)_4]$•xS (Cu-MOP) was obtained with a yield of 80% (**Figure 1**a and detailed preparation in the Supporting Information). Second, an Au NPs-based plasmonic substrate was prepared through a seed-based approach, and modified with 4-mercaptopyridine (4-PySH). Finally, the obtained plasmonic substrate was immersed into a DEF solution of Cu-MOP at room temperature. After 12 h immersion the substrate was rinsed with DEF and methanol thoroughly, and activated in vacuum at 60 °C. The resultant Cu-MOP-decorated plasmonic substrate was achieved through the coordination interaction between the axial Cu sites exposed outside of the Cu-MOP cage and the pyridine moieties attached on Au surface, and used for trace explosive sensing.

The structure of the Cu-MOP cage was determined by single-crystal X-ray analysis. As shown in Figure S1 and Tables S1 and S2 of the Supporting Information, the cage possesses a lantern-type structure arrangement with four bridging ligands surrounding two paddlewheel dicopper motifs, with a height of 19 Å and diameter of 26 Å, as well as an internal volume of $10.9 \times 10.7 \times 9.1$ Å^3. The electrospray ionization (ESI) measurement also confirmed the cage structure in solution. The ESI mass spectra (Figure 1b) of the Cu-MOP exhibited an intense peak at $m/z \approx 2063$, which could be assigned to the positively charged specie $[Cu_4(L\text{-}NH_2)_4]^+ Na^+$. It should be noted that the prepared Cu-MOP is an uncharged molecular cage. Compared to charged molecular cages (e.g., M. Fujita's coordination cages), it is quite difficult for the case of the uncharged molecular cages to achieve MS data with good quality.[8] In our case, in order to get the ESI-Mass data with good quality, we optimized the experiment conditions, including the spray voltage, capillary temperature, and ion accumulation time and finally achieved satisfied ESI results (Figure 1b). In addition, the scanning tunneling microscopy (STM) images in Figure S2 of the Supporting Information revealed the formation of ≈2 nm sized molecular particles, which is consistent with the size obtained by single-crystal X-ray analysis, further supporting the formation of the Cu-MOP cage.

The Au NPs-based plasmonic substrate was characterized by SEM. As shown in the inset of Figure 1c, the Au nanoislands clearly are formed on the substrate and separated by ≈10–100 nm gaps, exhibiting a suitable morphology for local electrical field enhancement and SERS for trace analyte sensing. As expected, the UV–vis absorption spectroscopy (Figure 1c) reveals a strong surface plasmon resonance at 525 nm typical for Au NPs in this size range. The modification of these Au islands with 4-PySH followed by further immobilization of the Cu-MOP cages was clearly confirmed by STM and XPS. In our case, for a better scanning image by STM an atomally flat Au (111) was used as substrate. Figure S3 of the Supporting Information shows the typical morphology of the self-assembled monolayer of 4-PySH (SAMs) on Au (111) surface. After the attachment of the Cu-MOP, the STM image (Figure S4, Supporting Information) reveals the cages homogeneously distributed on surface and the bright spots standing out demonstrate

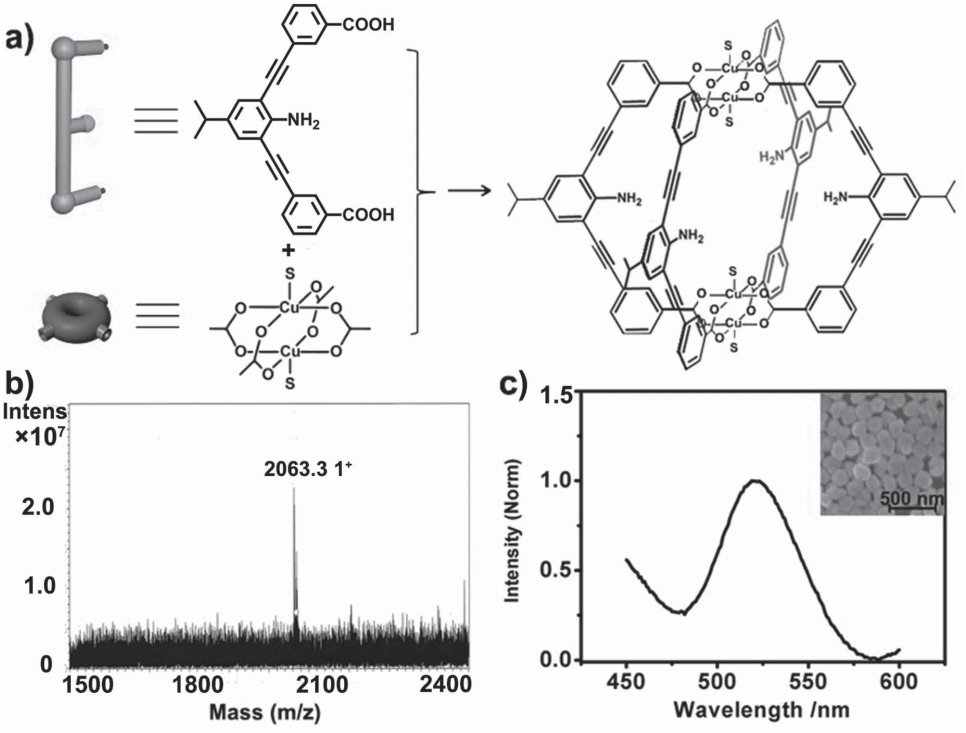

Figure 1. a) Schematic representation of the construction of Cu-MOP; S is the coordinated solvent molecule, which can be removed under a vacuum at 60 °C to yield an empty molecular cage for explosive trap; b) ESI spectrum of the Cu-MOP, showing an intense peak at m/z ≈ 2063, which could be assigned to the positively charged specie $[Cu_4(L\text{-}NH_2)_4]^+$ Na^+; c) UV–vis spectrum of the Au NPs-based plasmonic substrate; insert is the SEM image of the plasmonic substrate.

the regularity in size. By using XPS technique, we further confirmed the binding or grafting of 4-PySH and Cu-MOP onto the substrate. Figure S5a of the Supporting Information shows the XPS spectrum of 4-PySH modified substrate. The occurrence of C1s (284.81 eV), N1s (399.97 eV), S2p (161.99 eV), and Au4f (83.93 eV) bands indicates the presence of 4-PySH molecule on gold surface. Compared to the peak located at 163–164 eV for the unbound thiol species,[9a] in our case, the S2p peak is centered at 161.99 eV and can be assigned to the bound thiolate on gold surface,[9b,c] clearly proving that 4-PySH molecules were chemisorbed onto gold surface with the formation of Au–S bond. In addition, the peaks corresponding to free thiols were not observed, indicative of no trace of the starting material (4-PySH). After the attachment of Cu-MOP cages on the 4-PySH modified substrate, besides C1s, N1s, S2p, and Au4f bands, the Cu2p XPS signal was clearly detected at 932.21 eV (Figure S5a,b, Supporting Information), indicative of the successful grafting of the Cu-MOP cage onto the surface. Also, compared to the C1s spectrum of the 4-PySH modified substrate (Figure S5c, Supporting Information), which contains three different carbon atoms: the C=C (284.60 eV), the C—N (285.20 eV), and the C—S (286.14 eV), some new components were found in C1s spectrum for the case of the Cu-MOP treated substrate, as shown in Figure S5d, Supporting Information. With the help of literature,[9] these peaks could be assigned to the C≡C (283.92 eV), the C—NH_2 (287.39 eV), and the O—C=O (288.50 eV) species, clearly suggesting the successful grafting of Cu-MOP cages on the 4-PySH modified substrate. All these results corroborate a good grafting of 4-PySH and Cu-MOP cages on Au NPs-based plasmonic substrate.

SERS is an ultrasensitive vibrational spectroscopic technique for molecule sensing. Generally, the SERS enhancement factor is strongly related to the nanostructure of the used plasmonic substrate. In our work, a plasmonic substrate with desired morphology for strong local electrical field enhancement and SERS was fabricated by following Dai's method.[10] Based on the FDTD simulation, we found that a great localized surface plasmon resonance (LSPR) and substantial electromagnetic field enhancement could be achieved in the gaps between Au NPs, with a maximum enhancement up to 18-fold (**Figure 2**a,b). The variability in the background SERS signal of the Cu-MOP substrates without explosive was first examined. Figure S11 of the Supporting Information shows the comparison of the Raman spectra of the Cu-MOP substrates prepared in this work. The relative standard deviation (RSD) of major peaks is used to estimate the reproducibility of SERS signals. In our case, after the optimization of preparation conditions, the RSD value of the prepared Cu-MOP substrates is about 15.6%, which is consistent with the results of the Au NPs-based SERS substrates reported in the literature.[11a] Probably due to an inhomogeneous distribution of Au NPs, the background SERS signals vary to some extent. In fact, similar phenomenon was also found in the literature.[11b] Thus, it is expected that the Cu-MOP molecular cages anchored on the plasmonic substrate could serve as a unique receptor for sensitive detection of trace explosives.

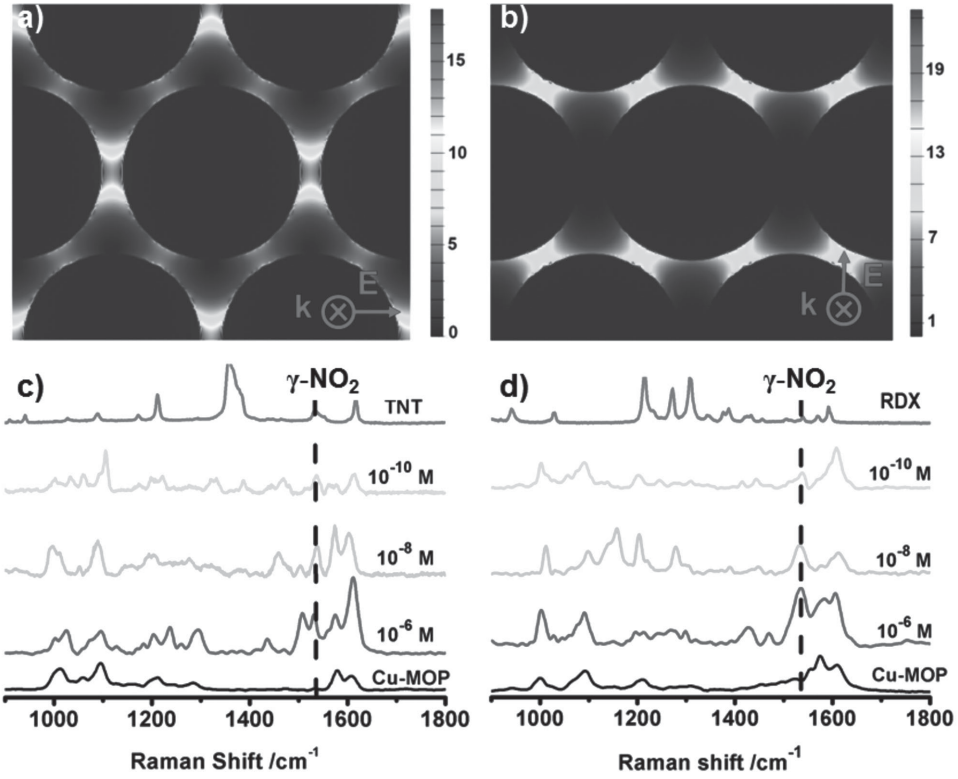

Figure 2. a) Distribution of the electric field intensity around Au NPs (d = 160 nm) at a wavelength of 633 nm; and b) the comparison of the SERS spectra for the Cu-MOP-modified substrate before and after exposure to c) TNT, or d) RDX solutions at different concentrations.

In our case, Cu-MOP-decorated plasmonic substrates were respectively immersed into the dichloromethane solutions of explosives with various concentrations for 6 h, and after thoroughly washing with dichloromethane the SERS spectra were collected (Figure 2c,d, and Figure S6, Supporting Information). The assignments of the peaks in the SERS spectra were summarized in Table S3 of the Supporting Information. As shown in Table S3 of the Supporting Information and Figure 2c, the trap of TNT molecule in Cu-MOP cage was detected, and the characteristic peaks of TNT at 1535 cm^{-1} (asymmetric nitro stretching), 1207 cm^{-1} (C–H ring bend and in-plane rocking), and 1613 cm^{-1} (2,6-NO_2, asymmetric ring stretching) appeared in the SERS spectrum at concentration of 10^{-6} M. Even if the concentration was down to 10^{-11} M, the characteristic vibration features could still be observable, indicative of an outstanding sensing capability. More strikingly, this superior sensing feature could be applied to detect the challenging aliphatic nitro-organics, such as RDX and HMX, as shown in Figure 2d and Figure S6, Supporting Information. Clearly, in the case of RDX, the asymmetric nitro group stretching band (1533 cm^{-1}) and the mainly methylene bending vibration modes with frequencies between 1340 and 1480 cm^{-1} (i.e., 1430 and 1472 cm^{-1}) containing N–N and NO_2 stretching could be observed. Also in the presence of HMX, the band in the region between 1200 and 1600 cm^{-1}, where the asymmetric stretch modes of nitro groups, wag of H atoms out of the CH_2 plane and the bend of H—C—H angles were also observed. As control experiments, Raman spectra of the used solid explosives (TNT, RDX or HMX) were collected and introduced in Figure 2, and Figures S6 and S10 of the Supporting Information, respectively. As shown in these figures, TNT, RDX, and HMX show the characteristic Raman peak of υNO_2 asymmetric stretching at 1535, 1533, 1538 cm^{-1}, respectively, which are consistent with the results in the literature.[12] Based on these results, we confirmed that the shoulder peak at ≈1535 cm^{-1} in the already existing signal is the signal of explosive compounds. In addition, the intensity of the shoulder peaks increase concomitantly with the increasing of the concentration of the exposed explosives (Figure S7, Supporting Information), further confirming our statement.

The algorithm used in the literature[13] was employed to determine the detection limits in our work. Concretely, the concentration response was quantified by observing the change in the ratio of the intensities of the Raman peaks (υNO_2) at ≈1535 cm^{-1} before and after the exposure of explosive compound. A series of experiments at different explosive concentrations was conducted and the results are plotted in Figure S7, Supporting Information. When monitoring the decrease in intensity at 1535 cm^{-1}, a clearly detectable response was observed at concentrations as low as 10^{-11} M for TNT and RDX, and 10^{-9} M for HMX.

The variability in the SERS response by using different batches of the Cu-MOP substrates in the presence of explosives was also examined. Figure S12 of the Supporting Information shows the comparison of the Raman spectra of the Cu-MOP substrates after the exposure to 10^{-6} M explosive (TNT, RDX or HMX). The RSD of major peaks is used to estimate the reproducibility of SERS signals. The RSD value for the case of TNT, RDX, and HMX is about 19.8%, 17.7%, and 16.8%, respectively,

which is consistent with the results of the Au NPs-based SERS substrates reported in the literature.[11a] Due to some variation of SERS responses from sample to sample as described above, we scaled back our claims of sensing limits. Thus, the sensing limits of 10^{-10} M for TNT and RDX, and 10^{-8} M for HMX were given in this work.

In the case of the larger explosive PETN, however, due to the presence of size-/shape-selectivity of the nature of Cu-MOP cage, no corresponding signals could be detected even after prolonged immersion time (Figure S8, Supporting Information). In our work the vibration modes which represent the $-NO_2$ asymmetric stretch of TNT, RDX, and HMX do not overlap with the bands of the 4-PySH layer and some of the normal vibrational bands of the above explosives seen at 1200–1500 cm^{-1} were absent in the spectra due to the formation of the space-confined host–guest complexes which results in restriction effects on the motions (vibrations, torsions, etc.) of the explosive inside the cavity, and thus leads to the distinct behaviors from bulk liquid phases.[14] Note that the trap of guest molecules inside host molecule with multiple interactions would have a significant effect on the Raman spectra and thus results in the broadening of the related Raman spectra.[15] Compared with the reported $-NH_2$ modified plasmonic counterparts,[16] which show only moderate interactions with the above explosives, the detection limits of our Cu-MOP-modified plasmonic substrates are several orders of magnitude lower. These results indicate that the formation of a host-stabilized binary complex is critical for the good sensing of explosives. As a blank experiment, the Cu-MOP-modified plasmonic substrate was also exposed to the used solvent CH_2Cl_2. In Figure S10d of the Supporting Information, no change was observed in the SERS spectrum, indicating that the changes in the SERS spectra described above were not due to the solvent effect. Importantly, we found that the trapped explosive molecules inside Cu-MOP could be removed by washing with methanol and dichloromethane and activated in vacuum at 60 °C, indicating the sensing ability of the constructed substrates is completely regenerable (Figure S10, Supporting Information).

To facilitate an intuitive understanding of our sensing system, the molecular sizes of explosive molecules and Cu-MOP cage were calculated and provided in Table S2 of the Supporting Information. Clearly, due to the large size of RDX and HMX, only one explosive molecule could be trapped inside Cu-MOP cage. To better understand the nature of the interactions between the explosives and the Cu-MOP host and to reveal the related trap effect, we conducted ESI-Mass studies. As shown in Figure S13of the Supporting Information, in the case of a solution of Cu-MOP in the presence of an equimolar amount of explosive TNT, an intense peak at m/z ≈ 2295.73 appears, which could be assigned to $[Cu_4(L\text{-}NH_2)_4 \cdot TNT]$, thus evidencing a 1:1 stoichiometric host–guest complexation. For the cases of RDX and HMX, the similar patterns in Figures S14 and S15 of the Supporting Information also indicate that the Cu-MOP receptor indeed possesses a suitable cavity to capture one guest molecule. The inclusion phenomenon was further characterized by means of UV/vis measurements (**Figure 3**a). Clearly, the Cu-MOP exhibits ligand-based charge–transfer bands at 258 nm in DEF solution.[17a] Upon the addition of RDX or HMX the intensity of absorption at 258 nm increases while TNT causes a significant decrease in the intensity of the absorption at 388 nm and the occurrence of a new band at 465 nm (Figure 3a and Figure S16, Supporting Information).

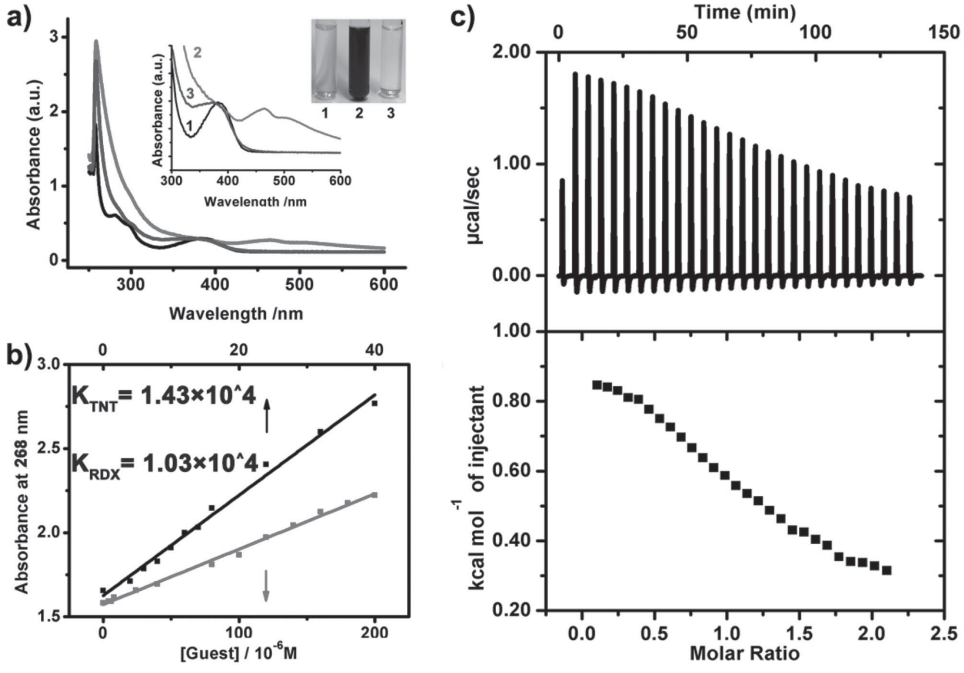

Figure 3. a) Comparison of the UV–vis spectra of the Cu-MOP and the formed Cu-MOP•explosive complex in DEF solvent (1: Cu-MOP; 2: TNT@Cu-MOP; 3: RDX@Cu-MOP); b) plots of the absorbance at 268 nm (A268) versus the concentration of guest (TNT and RDX) in DCM solution, and the fitting of the data to a 1:1 binding model allowed a determination of $K_{TNT} = 1.43 \times 10^4$ M^{-1} and $K_{RDX} = 1.03 \times 10^4$ M^{-1}; c) ITC data for the titration of Cu-MOP (0.4×10^{-3} M) with TNT (4×10^{-3} M) in DEF solvent at 25 °C.

We proposed that the new band for the case of TNT could be attributed to the charge–transfer interaction between the $-NH_2$ moieties of the cage and the TNT. The binding mechanism is similar to that of the previous report[17b] and also the addition of TNT into the Cu-MOP solution causes the color change from colorless to deep red. For the case of RDX, two isosbestic points appear at 378 and 413 nm, indicative of the prospective guest binding within the molecular cage. The individual profile of RDX and HMX (Figure 3b and Figures S17 and S18, Supporting Information) of the bands at 258 nm further demonstrated the occurrence of 1:1 stoichiometric host–guest complexations with the association constants (log K_{ass}) of 4.01 for RDX and 3.20 for HMX. Additionally, isothermal titration calorimetry (ITC) was used for determine the thermodynamic parameters for the combination of Cu-MOP and explosive molecules. A 1:1 binding stoichiometry was observed for the explosive TNT. The ITC data (Figure 3c, Table S5, Supporting Information) showed a moderate affinity ($K_a = 1.05 \times 10^3$). However, for the cases of RDX and HMX, the ITC experiments failed, due to little heat change and large heat of dilution during the titration process.

Only the SERS data are not convincing enough to conclusively prove the encapsulation of the explosives in the MOP cages grafted onto the substrate. Thus, the control experiment and FT-IR measurements were also performed to further confirm the guest binding of the MOP cages on the solid substrate. As a control experiment, the same plasmonic substrate only without the grafted Cu-MOP cage was exposed to the targeted solutions under the same conditions. No explosives were detected in SERS spectra (Figure S9, Supporting Information), indicating that the observed SERS signals of explosives in the case of the Cu-MOP-decorated substrates should arise from the binding interaction between the MOP cages and explosive molecules. FT-IR measurements further confirmed the presence of the binding interaction between the MOP cages and explosives, and the characteristic absorption bands of explosives were observed (Figure S19, Supporting Information). Importantly, compared to the corresponding explosives, due to the confinement effect from the MOP cage, the vibration and stretching of explosive molecule inside cage were restricted,[14] and thus some typical bands were deeply decreased in intensity, and some vibration bands disappeared. All these above results indicate that the explosive molecule was actually trapped or encapsulated in the MOP cavities. Single-crystal X-ray diffraction can provide direct elucidation of the host–guest interaction at molecular level. Unfortunately, all attempts to obtain the corresponding single crystals of explosive molecule in Cu-MOP failed. However, from the PXRD patterns of the Cu-MOP cages with bound explosives (Figure S20, Supporting Information), it can be seen that the presence of explosives did not change the packing behavior of the Cu-MOP cage. A DFT computational study was carried out to understand the host–guest interactions. DFT-D2 method was adopted to consider the van der Waals interactions.[18] The detailed calculation was shown in the Supporting Information. As shown in Figure S21 of the Supporting Information, the molecular structures from single crystal and DFT calculations agreed well with each other. **Figure 4**, and Figures S22 and S23 of the Supporting Information show the molecular structure of the binary complexes. In view of the geometrical accommodation evidenced from the DFT calculation, the binary complex should adopt a 1:1 stoichiometry, which confirms our experiment results. The binding energies of the molecules trapped in the Cu-MOP cage are summarized in **Table 1**. In comparison with a typical adsorbent-adsorbate system, such as CO_2 in zeolite,[19] the magnitude of the binding

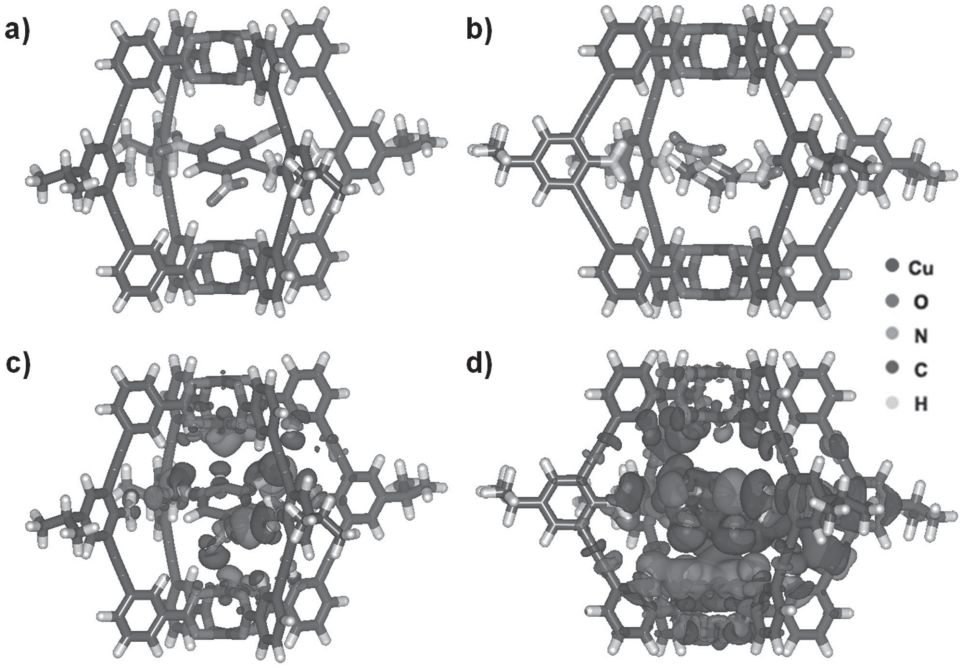

Figure 4. Simulated locations of a) TNT and b) RDX molecule in Cu-MOP cage; Difference-electron density of c) TNT@Cu-MOP and d) RDX@Cu-MOP complex. Blue constant-density surfaces (iso-surfaces) represent electron depletion region and red surfaces represent electron accumulation region.

Table 1 Charge transfer to Cu and $-NH_2$ of Cu-MOP upon adsorption of explosive molecules (TNT, DNT, RDX, and HMX) using the DDEC method[22] and the corresponding binding energy. All charge–transfer values are given in electron charge.

	Cu^{2+}	$-NH_2$	Binding energy [eV]
Cu-MOP	–	–	–
DNT@Cu-MOP	−0.024	−0.020	−0.75
TNT@MOP	−0.035	−0.023	−0.84
RDX@MOP	−0.091	−0.009	−1.20
HMX@MOP	−0.150	−0.006	−1.25

energies suggests a strong affinity of Cu-MOP cage for TNT, DNT, RDX, or HMX, which is consistent with the good sensing of the Cu-MOP to these explosives.

To understand the strong affinity of Cu-MOP cage, in-depth analyses were performed. In the case of DNT@Cu-MOP, the two NO_2^- groups directly point toward two NH_2^+ in the cage with the nearest O–H interatomic distances are 2.30 and 2.34 Å, respectively (**Figure 5**a). Such donor–acceptor distance falls in the "strong, mostly covalent" category of a hydrogen bond.[20] For the TNT@Cu-MOP, two NO_2^- groups of TNT molecule direct two NH_2^+ groups of Cu-MOP, respectively, while the third NO_2^- points toward between two NH_2^+ groups (Figure 5b), with the line formed by the four Cu^{2+} of the Cu-MOP penetrating the "central ring" of the TNT molecule (Figure 4a). The interatomic O–H distances (Figure 5b) suggests four binding sites between Cu-MOP and TNT. In the case of RDX@Cu-MOP and HMX@Cu-MOP (Figure 5c,d), the number of binding sites increases to 4 and 5, respectively.

In addition, difference-electron density results in Figure 4c,d and density-derived electrostatic chemical net atomic charge (DDEC) results reveal the occurrence of significant charge transfers between the Cu-MOP cage and the trapped molecules (Table 1). Specifically, TNT loses electrons to the adjacent Cu atoms of Cu-MOP, with the maximum charge transfer to a single Cu of −0.035; at the same time TNT loses electrons to all the NH_2^+ groups but of smaller magnitude with the maximum charge transfer to a single NH_2^+ of −0.023. Compared with TNT, RDX exhibits stronger charge transfer to the Cu ion (−0.091) and weaker charge transfer to the NH_2^+ groups (−0.0009). As for the rest two explosive molecules, DNT behaves similar to TNT while HMX similar to RDX. In all cases, the charge transfer to Cu ions is more profound than the NH_2^+. It should be noted that DFT calculations and the UV–vis measurements seem to provide conflicting binding story. The main reason for this phenomenon is that the UV–vis measurements were performed in the presence of solvents while the DFT calculations were carried out in vacuum. The experimental and theoretical binding energies cannot be directly compared due to the neglect of solvation effects in the calculations.[21a] Solvent has significant effects on guest binding and dynamics of a host molecular cage.[21b]

As shown in Table 1, the binding energies of the binary complexes correlate very well with the number of binding sites and the charge transfer from the trapped molecules to Cu^{2+} and NO_2^- groups. The cage topology not only enhances the number of binding sites between NO_2^- and NH_2^+ but also provides additional binding contributions from the Cu^{2+} ions. We contend that such multiple weak interactions give rise to the formation of a host-stabilized binary complex. These results described

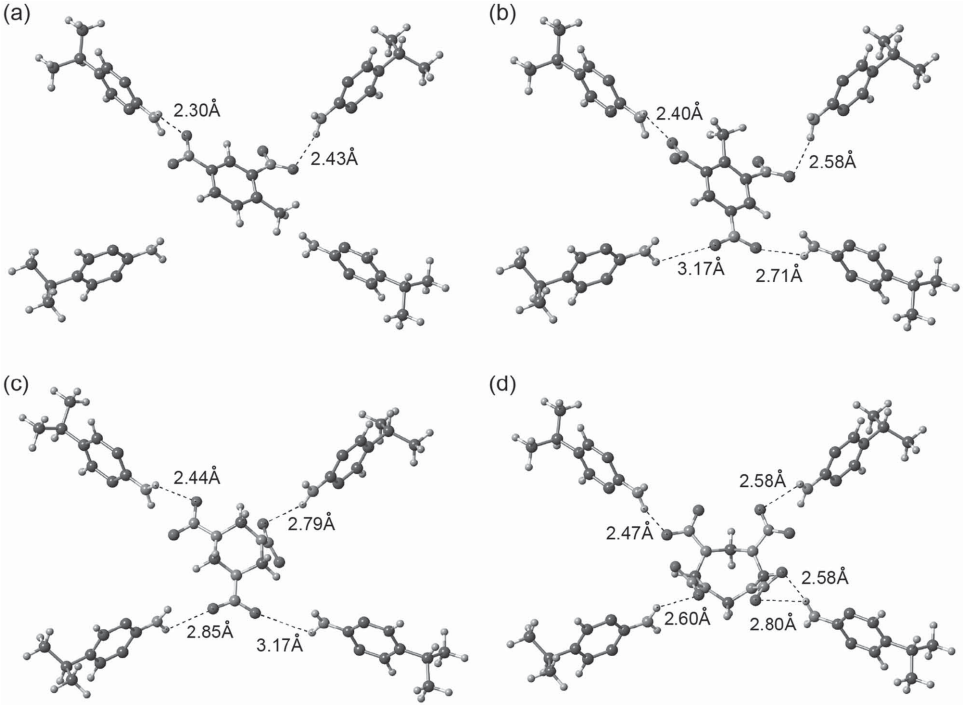

Figure 5. Simulated geometries of explosive molecules in Cu-MOP: a) DNT@Cu-MOP; b) TNT@Cu-MOP; c) RDX@Cu-MOP; d) HMX@Cu-MOP.

above are encouraging. Based on the unique confinement effect and the size-/shape-exclusion of the Cu-MOP cage grafted onto a plasmonic substrate, direct detection and discrimination of distinctively different classes of trace explosives in solution are realized by using one molecular cage, especial the challenging aliphatic nitro-organics RDX and HMX. The key point of this sensing protocol is the rational integration of multiple weak molecular interactions inside the molecular cage cavity and the cooperation of substrate with good SERS enhancement factor. Compared with the explosive sensors reported, our constructed sensor also exhibited a good sensitivity. Currently, establishing a practical sensing platform for molecular recognition with high sensitivity and selectivity, with the ultimate goal of detecting single-molecule events, is of great importance to chemical analysis. We believe that our created sensing platform could be a universal platform for trace analyte sensing. By careful selecting MOP cage and optimizing the structure of plasmonic substrate, we may ultimately achieve the selective sensing of ultratrace explosives, or even single-explosive molecule. The related work is ongoing in our lab.

3. Conclusion

In conclusion, based on the MOP cage-decorated plasmonic substrate, a novel strategy for selective, fully reversible, and highly sensitive detection of broad class of explosives, including the most challenging explosives such as RDX and HMX, has been developed. Such outstanding sensing features are on one hand attributed to the cooperation of plasmonic nanohybrid substrate with a good SERS enhancement factor, and on the other hand benefited from the rational integration of multiple weak molecular interactions inside the molecular cage, providing multiple guest-accessible interaction sites and thus offering an efficient communicator that is able to amplify the host–guest event. Moreover, the pore and window size of MOP cage could be efficiently modulated to allow a size or/and shape selectivity toward special explosives. Compared with those sophisticated nitro-organics sensors, we believe our strategy can be further extended to other specific analytes, which may be difficult to recognize with conventional methods. Therefore, our findings would open a new way to design and develop a new sensing platform to enable broad applications in a wide range.

4. Experimental Section

Synthesis of MOP: MOP can be synthesized by the direct reaction between $Cu_2(OAc)_4{\cdot}H_2O$ and 3,3-(2-Amino-5-iso-propyl-1,3-phenylene)-bis(ethyne-2,1-diyl)dibenzoic acid (L-NH_2). Both reactants dissolved in 2 mL DEF ($Cu_2(OAc)_4{\cdot}H_2O$: L-NH_2 = 1:1, [L-NH_2] = 0.025 M) were mixed and then 2 mL MeOH was added upon the resulting solution, after 5 d, green crystals were harvested (80% yield based on $Cu_2(OAc)_4{\cdot}H_2O$). FTIR (neat, cm^{-1}): 3471(m), 3371(m), 2972(m), 2196(w), 1657(w), 1619(m), 1590(w), 1565(m), 1473(m), 1430(m), 1391(s), 1304(w), 1266(w), 1237(w), 1211(w), 1164(w), 1115(w), 1067(m), 999(w), 916(m), 879(m), 825(w), 796(m), 762(s), 680(m), 545(m), 492(m).

Data center: CCDC 1036808 (Cu -MOP).

The data can be obtained free of charge from The Cambridge Crystallographic Data Center via www.ccdc.cam.ac.uk/data_request/cif.

Preparation of Sensing Substrate and Sensing Procedure: The size of constructed sensing substrate is >> 1 × 1 cm^2. A three-step procedure was employed to construct the MOP-decorated plasmonic nanohybrid substrate. First, the MOP cage was synthesized by slow addition of methanol onto a DEF solution of $Cu_2(OAc)_4$ and ligand H2(2-NH2-5-i-Pr-3,3¢-PBEDDB) (L-NH_2). After 3 d the MOP cage $[Cu_4(L\text{-}NH_2)_4(S)_4]{\bullet}xS$ (Cu-MOP) was synthesized with a yield of 80% (detailed preparation in the Supporting Information). Second, the Au NPs-based plasmonic substrate was prepared through a seed-based approach, and modified with 4-mercaptopyridine (4-PySH). Finally, the obtained plasmonic substrate was immersed into a DEF solution of Cu-MOP at RT. After 12 h immersion the substrate was rinsed with DEF and methanol, and activated in vacuum at 60 °C.

For the sensing experiment, the activated plasmonic substrates were respectively immersed into the dichloromethane solutions of explosives with various concentrations for 6 h, and after thoroughly washing with dichloromethane the SERS spectra were collected. For the regenerable sensing experiment, after the first sensing, the trapped explosive molecules inside Cu-MOP was removed by washing with methanol and dichloromethane and the substrate was activated in vacuum at 60 °C, then the substrate was used for the second sensing.

Supporting Information

Supporting Information is available from the Wiley Online Library or from the author.

Acknowledgements

C.W. and J.S. contributed equally to this work. The authors acknowledge the financial support from the NSFC (50873051 and 205333050), MOST (2007AA03Z307), and Transregional Project (TRR61). The authors also thank Dr. G. Wu and Prof. Xi Zhang at Tsinghua University for useful discussion and the ITC measurement.

Received: July 24, 2015
Published online: August 31, 2015

[1] a) S. W. Thomas, G. D. Joly, T. M. Swager, *Chem. Rev.* **2007**, *107*, 1339; b) D. T. McQuade, A. E. Pullen, T. M. Swager, *Chem. Rev.* **2000**, *100*, 2537; c) Y. Che, D. E. Gross, H. Huang, D. Yang, X. Yang, J. S. Moore, L. Zang, *J. Am. Chem. Soc.* **2012**, *134*, 4978; d) J. C. Sanchez, W. C. Trogler, *J. Mater. Chem.* **2008**, *18*, 3143.

[2] a) Y. Salinas, R. Martínez-Máñez, M. D. Marcos, F. Sancenón, A. M. Costero, M. Parra, S. Gil*Chem. Soc. Rev.* **2012**, *41*, 1261; b) A. Lan, K. Li, H. Wu, D. H. Olson, T. J. Emge, W. Ki, M. Hong, J. Li, *Angew. Chem. Int. Ed.* **2009**, *48*, 2334.

[3] a) T. L. Andrew, T. M. Swager, *J. Am. Chem. Soc.* **2007**, *129*, 7254; b) S. Pramanik, C. Zheng, X. Zhang, T. J. Emge, J. Li, *J. Am. Chem. Soc.* **2011**, *133*, 4153; c) M. E. Germain, M. J. Knapp, *J. Am. Chem. Soc.* **2008**, *130*, 5422.

[4] W. Zhu, W. N. Li, C. Wang, J. C. Cui, H. W. Yang, Y. Jiang, G. T. Li, *Chem. Sci.* **2013**, *4*, 3583.

[5] a) J. R. Li, H. C. Zhou, *Nat. Chem.* **2010**, *2*, 893; b) D. Fujita, K. Suzuki, S. Sato, M. Yagi-utsumi, Y. Yamaguchi, N. Mizuno, T. Kumasaka, M. Takata, M. Noda, S. Uchiyama, K. Kato, M. Fujita, *Nat. Commun.* **2012**, *3*, 1093.

[6] C. He, Z. H. Lin, Z. He, C. Y. Duan, C. H. Xu, Z. M. Wang, C. H. Yan, *Angew. Chem. Int. Ed.* **2008**, *47*, 877.

[7] D. Zhao, S. Tan, D. Yuan, W. Lu, Y. H. Rezenom, H. Jiang, L. Q. Wang, H. C. Zhou, *Adv. Mater.* **2011**, *23*, 90.

[8] Q. L. Zou, L. Zhang, X. H. Yan, A. H. Wang, G. H. Ma, J. B. Li, H. Möhwald, S. Mann, *Angew. Chem. Int. Ed.* **2014**, *53*, 5842.

[9] a) E. A. Ramírez, E. Cortés, A. A. Rubert, P. Carro, G. Benítez, M. E. Vela, R. C. Salvarezza, *Langmuir* **2012**, *28*, 6839; b) H. L. Zhang, S. D. Evans, J. R. Henderson, R. E. Miles, T. H. Shen, *J. Phys. Chem. B* **2003**, *107*, 6087; c) M. Gosecka, J. Pietrasik, P. Decorse, B. Glebocki, M. M. Chehimi, S. Slomkowski, T. Basinska, *Langmuir* **2015**, *31*, 4853; d) J. Q. Zhao, C. H. Lu, X. He, X. F. Zhang, W. Zhang, X. M. Zhang, *ACS Appl. Mater. Interfaces* **2015**, *7*, 2607.

[10] S. M. Tabakman, Z. Chen, H. S. Casalongue, H. L. Wang, H. J. Dai, *Small* **2011**, *7*, 499.

[11] a) C. L. Zhang, K. P. Lv, H. P. Cong, S. H. Yu, *Small* **2012**, *8*, 648; b) B. H. Zhang, H. S. Wang, L. H. Lu, K. L. Ai, G. Zhang, X. L. Cheng, *Adv. Funct. Mater.* **2008**, *18*, 2348.

[12] a) H. V. Brand, R. L. Rabie, D. J. Funk, I. Diaz-Acosta, P. Pulay, T. K. Lippert, *J. Phys. Chem. B* **2002**, *106*, 10597; b) S. Sil, D. Chaturvedi, K. B. Krishnappa, S. Kumar, S. N. Asthana, S. Umapathy, *J. Phys. Chem. A* **2014**, *118*, 2904.

[13] A. Ingram, L. Byers, K. Faulds, B. D. Moore, D. Graham, *J. Am. Chem. Soc.* **2008**, *130*, 11846.

[14] a) S. Hashimoto, T. Fujimori, H. Tanka, *J. Am. Chem. Soc.* **2011**, *133*, 2022; b) L. Marchese, A. Frache, E. Gianotti, G. Martra, M. Causà, S. Coluccia, *Microporous Mesoporous Mater.* **1999**, *30*, 145.

[15] M. Erol, Y. Han, S. K. Stanley, C. M. Stafford, H. Du, S. Sukhishvili, *J. Am. Chem. Soc.* **2009**, *131*, 7480.

[16] O. J. Glembocki, M. Gowda, S. Geng, S. M. Prokes, N. Y. Garces, J. Cushen, J. D. Caldwell, *Plasmonics: Met. Nanostruct. Opt. Prop. VIII* **2010**, *7757*, 77570I–1-.

[17] a) E. W. Wilson, M. H. Kasperian, R. B. Martin, *J. Am. Chem. Soc.* **1970**, *92*, 5365; b) Y. Engel, R. Elnathan, A. Pevzner, G. Davidi, E. Flaxer, F. Patolsky, *Angew. Chem. Int. Ed.* **2010**, *49*, 6830.

[18] S. Grimme, *J. Comput. Chem.* **2006**, *27*, 1787.

[19] J. Shang, G. Li, R. Singh, P. Xiao, D. Danaci, J. Z. Liu, P. A. Webley, *J. Phys. Chem. C* **2013**, *117*, 12841.

[20] G. A. Jeffrey, *An Introduction to Hydrogen Bonding*, Oxford University Press, **New York 1997**.

[21] a) C. Márquez, R. R. Hudgins, W. M. Nau, *J. Am. Chem. Soc.* **2004**, *126*, 5806; b) J. L. Bolliger, T. K. Ronson, M. Ogawa, J. R. Nitschke, *J. Am. Chem. Soc.* **2014**, *136*, 14545.

[22] a) T. A. Manz, D. S. Sholl, *J. Chem. Theory Comput.* **2010**, *6*, 2455; b) T. A. Manz, D. S. Sholl, *J. Chem. Theory Comput.* **2011**, *7*, 4146; c) T. A. Manz, D. S. Sholl, *J. Chem. Theory Comput.* **2012**, *8*, 2844.